Exploring Strategies Towards Synthetic Precision Control within Core-shell Nanowires

Kenna L. Salvatore and Stanislaus S. Wong*

Email: stanislaus.wong@stonybrook.edu

Department of Chemistry, State University of New York at Stony Brook, Stony Brook, NY 11794-3400

*To whom correspondence should be addressed.

Conspectus: Achieving precision and reproducibility in terms of physical structure and chemical composition within arbitrary nanoscale systems remains a 'holy grail' challenge for nanochemistry. Because nanomaterials possess fundamentally distinctive size-dependent electronic, optical, and magnetic properties with wide-ranging applicability, the ability to produce homogeneous and monodisperse nanostructures with precise size and shape control, while maintaining a high degree of sample quality, purity, and crystallinity, remains a key synthetic objective. Moreover, it is anticipated that the methodologies developed to address this challenge ought to be reasonably simple, scalable, mild, non-toxic, high-yield, and cost-effective, while minimizing reagent use, reaction steps, byproduct generation, and energy consumption.

The focus of this Perspective Account revolves around the study of various types of nanoscale one-dimensional core-shell motifs, prepared by our group. These offer a compact structural design, characterized by atom economy, to bring together two chemically distinctive (and potentially sharply contrasting) material systems into contact within the structural context of an extended, anisotropic configuration. Herein, we describe complementary strategies aimed at resolving the aforementioned concerns about precise structure and compositional control through the infusion of careful 'quantification' and systematicity into customized, reasonably sustainable nanoscale synthetic protocols, developed by our group. Our multi-pronged approach involved the

application of (a) electrodeposition, (b) electrospinning, (c) a combination of underpotential deposition and galvanic displacement reactions, and (d) microwave-assisted chemistry to diverse core-shell model systems, such as (i) carbon nanotube – SiO₂ composites, (ii) SnO₂/TiO₂ motifs, (iii) ultrathin Pt-monolayer shell-coated alloyed metal core nanowires, and (iv) Cu/TiO₂ nanowires, for applications spanning optoelectronics, photocatalysis, electrocatalysis, and thermal CO₂ hydrogenation, respectively.

In so doing, over the years, we have reported on a number of different characterization tools involving spectroscopy (e.g., extended X-ray absorption fine structure (EXAFS) spectroscopy) and microscopy (e.g., high-resolution transmission electron microscopy (HRTEM) and atomic force microscopy (AFM)) for gaining valuable insights into the qualitative and quantitative nature of not only the inner core and outer shell themselves but also their intervening interface. While probing the functional catalytic behavior of a few of these core-shell structures under realistic operando conditions, using dynamic, in situ characterization techniques, we found that local and subtle changes in chemical composition and physical structure often occur during the reaction process itself. As such, subtle differences in atomic packing, degree of derivatization, defect content, and/or extent of crystallinity can impact upon observed properties with tangible consequences for performance, mechanism, and durability.

Key References:

- Kenna L. Salvatore, Kaixi Deng, Shiyu Yue, Scott C. McGuire, José A. Rodriguez, and Stanislaus S. Wong, "Optimized Microwave-based Synthesis of Thermally-Stable Inverse Catalytic Core-Shell Motifs for CO₂ Hydrogenation", ACS Applied Materials and Interfaces, 12(29), 32591-32603 (2020). The reliable production of Cu@TiO₂ core@shell nanowire (NW) structures using a microwave-assisted method for CO₂ hydrogenation was thoroughly investigated. Specifically, we modified a significant range of experimental parameters, including (i) controlled variation in molar ratios, (ii) the identity of the Ti precursors, (iii) the method of addition of the precursors, and (iv) irradiation time.
- Haiqing Liu, Wei An, Yuanyuan Li, Anatoly I. Frenkel, Kotaro Sasaki, Christopher Koenigsmann, Dong Su, Rachel M. Anderson, Richard M. Crooks, Radoslav R. Adzic, Ping Liu, and Stanislaus S. Wong, "In situ Probing of the Active Site Geometry of Ultrathin Nanowires for the Oxygen Reduction Reaction", J. Am. Chem. Soc., 137(39), 12597–12609 (2015). We probed ultrathin core—shell Pt~Pd9Au nanowires, from the complementary perspectives of both DFT calculations and X-ray absorption spectroscopy (XAS). Taken collectively, the combination and reconciliation of complementary data from both experimental and theoretical studies revealed that the catalytically active structure of our ternary nanowires, responsible for the observed performance enhancements in the oxygen reduction reaction, could actually be ascribed to an unanticipated PtAu~Pd configuration. This structure was comprised of a PtAu binary shell coupled with a pure inner Pd core, whose formation was attributable to a specific synthesis step, namely Cu underpotential deposition (UPD) followed by galvanic replacement with Pt.

- Xiaohui Peng, Alexander C. Santulli, Eli Sutter, and Stanislaus S. Wong, "Fabrication and Enhanced Photocatalytic Activity of Inorganic Core-shell Nanofibers Produced by Coaxial Electrospinning", Edge Article, Chemical Science, 3(4), 1262 1272 (2012). Uniform SnO₂/TiO₂ coaxial nanoscale fibers with a tunable internal morphology were prepared in one step using coaxial electrospinning. By predictively changing the concentration of the tin precursor solution, the internal structures of these fibers could be reliably tuned from filled solid structures to peapod-like motifs, and even to hollow tubes.
- Mandakini Kanungo, Hugh S. Isaacs, and Stanislaus S. Wong, "Quantitative Control over Electrodeposition of Silica films onto Single-Walled Carbon Nanotube Surfaces", invited contribution (Richard E. Smalley Memorial issue), *J. Phys. Chem. C*, 111(48), 17730-17742 (2007). We developed two viable and methodical means with which to coat carbon nanotubes with various discrete and quantifiable thicknesses of silica using an electrochemical sol-gel process, run under relatively mild reaction conditions. The thickness of the silica coating could be controllably adjusted by varying not only the potential of the working electrode but also the concentration of the sol solution.

1. Introduction

One of the grand challenges in nanoscience is to reliably create nanomaterials with a high level of chemical precision and confidence coupled with an intimate and well-defined understanding of molecular bonding, as is commonly expected of complex molecules generated by a conventional organic synthesis, as an illustrative example. The expectation for nanoscience, which remains to be realized in a broader sense, is to routinely fabricate monodisperse nanostructures with precise size and shape control, while simultaneously achieving high sample quality, purity, and crystallinity.

Moreover, the idea of being able to rationally design nanomaterials with tunable properties (and hence structure-property correlations) remains an appealing synthetic objective in nanochemistry. In this context, an ongoing objective within our group has been to generate effective, sustainable protocols with the goal of producing more complicated multi-atom, nanoscale architectures and heterojunctions, which can be similarly probed and defined at the molecular level using a suite of advanced characterization tools. 1-4 Specifically, the goal of synthesizing heterostructures and variants thereof is to combine the favorable attributes of individual, distinctive atoms into an integrated unit with often unique and distinctive properties. 5,6

As an illustrative example of our work in enabling this desired outcome, we have reported on the production of segmented Pd/Pt and Pd/Au nanowires (NWs), incorporating two spatially segregated, chemically dissimilar, but elementally pure, axial subunits, with reliable and predictive control over their relative constituent unit lengths. These segmented NWs, which we explored as both electrocatalysts and nanomotors, consisted of a fusion of high-quality, crystalline, elementally pure sub-units, individually separated by well-defined interfaces between the constituent metals. Core-shell Systems: Herein in this Account, we focus on a specific class of nanoscale motifs, namely core-shell 1D NW-based architectures. As justification for our interest in these systems, 1D

nanomaterials often are characterized by robust mechanical strength, advantageous structural flexibility, and the favorable exposure of relatively large surface areas of promising reactivity. 8 The quantum confinement effect⁸ within these anisotropic materials means that 1D nanostructures represent the smallest-dimensional motifs, capable of promoting the effective, unimpeded transport of electrons and optical excitations. Structurally, single-crystalline 1D nanostructures maintain (a) high aspect ratios, (b) relatively fewer lattice boundaries, (c) uninterrupted segments of smooth crystalline planes, and (d) a low number of defect sites. ¹⁰ In principle, the surfaces of 1D morphologies can be tuned so as to preferentially evince specific crystal facets. 11 As such, 1D coreshell motifs offer a compact design, comprised of an outer shell of one composition circumscribing an inner core of a different makeup, within the context of an extended anisotropic configuration. Relevant Synthesis Protocols. In general, a core-shell heterostructure can be generated using twostep synthetic protocols, wherein an inner one-dimensional core template is initially pre-formed after which an external shell coating is subsequently introduced. 12 The fundamental issue is that generating novel two-step synthetic protocols through a permutation of the different, conventionally used methods is complicated by the need to overcome the inherent limitations associated with each individual synthesis technique, incorporated into the overall process. ¹³ As such, developing meaningful, facile, and practical 'quasi-one-step' protocols using simple, scalable, and sustainable methods, which can be readily construct discrete, monodisperse 1D core-shell nanostructures incorporating two materials of arbitrary chemical compositions, still remains a significant and nontrivial synthetic challenge. That is, how can one demonstrate precise (and potentially quantifiable) structural control within this important family of architectures?

Therefore, over the years, our group has explored a number of diverse, complementary ideas that have sought to address this basic problem by applying (a) electrodeposition, (b) electrospinning,

(c) a combination of underpotential deposition (UPD) and galvanic displacement (GD) reactions, and (d) most recently, microwave-assisted chemistry, respectively, to various core-shell systems for diverse applications (Figure 1). It is apparent that a number of these techniques utilize facile electrochemistry and/or the application of electric fields or a combination thereof. Moreover, we have used different characterization strategies for achieving meaningful insights into the nature of not only the core and shell themselves but also the intervening interface lying in between. Our objective in these diverse efforts has been to correlate rational parameter control with an understanding of the resulting chemical composition and physical structure. In particular, we have been concerned with tuning the magnitude of the thickness of the outer shell, which can have important and potentially unforeseen ramifications for both physical and chemical properties.

2. Synthesis Methods

While individually effective in fabricating 1D core@shell architectures, the various synthesis protocols discussed herein, such as electrodeposition, electrospinning, UPD/GD, and microwave-assisted methods, are inherently dissimilar in nature. Each process maintains its own singular advantages and disadvantages, many of which are highlighted in Table 1.

As an example, electrodeposition obviates the need for either surfactants or reducing agents, which can potentially interfere with catalytic performance; moreover, this procedure is reasonably simple to implement, involves relatively fast reaction times, and provides for reliable, precise, and reproducible control over composition and structure. Specifically, reaction parameters, such as the magnitude of the applied voltage, the magnitude of the precursor concentration, and the deposition time allow for tunable control of the shell size. Nevertheless, the viability of electrodeposition, which depends on the application of an external electric field to facilitate redox reactions, is fundamentally constrained by (i) its poor yields, (ii) potential for enabling surface aggregation, and

(iii) requirement of a relatively conductive substrate and precursor, all of which can collectively limit the range of applicable material systems that can be generated with this method.¹⁴

By contrast, electrospinning represents a relatively straightforward, energetically sustainable, and effective means for producing highly uniform 1D nanofibers of either polymeric or inorganic-based composites. ¹⁵ Its positive attributes include not only its high continuous throughput under relatively mild conditions but also its innate capability to flexibly dictate the dimensions of the resulting fiber from the micron to the nanometer range. ¹⁶ With the development of the coaxial nozzle, thereby enabling the simultaneous electrospinning of two different components, ¹⁷ it became feasible to prepare 1D core-shell nanoscale heterostructures on a large scale within a one-step synthetic process. Indeed, the benefits of using coaxial electrospinning as a viable means to fabricate 1-D heterostructures with different compositions and configurations were associated with its (a) enviable flexibility in terms of potential material choices with implications for incorporating desirable functionalities, (b) attractive synthetic simplicity, reliability, low cost, and (c) high yield. ¹⁸ However, the disadvantages of this technique can be attributed to issues, associated with either the chemical compatibility or solvent miscibility of the precursors and resulting products. Moreover, apparent yields can be impacted by local technical concerns, such as nozzle clogging. ¹⁶

Third, the combination of UPD and GD optimized by our group for 1D motifs represents a specialized type of electrodeposition. In our overall process for producing Pt-coated NWs, a Cu monolayer (ML) is initially deposited by linear sweep voltammetry at a potential of ~0.5 V. This step occurs by a two-electron cathodic reduction atop the electrode surface itself. The rapid scan rate allows for the deposition of a single ML without bulk deposition. The ML-modified electrode is subsequently immersed in H₂PtCl₆ and due to a favorable potential for the overall galvanic exchange process, the Cu is spontaneously displaced by Pt, thereby yielding a reduced elemental Pt ML.

Whereas our UPD/GD protocol is reproducible, provides for reliable control over shell thickness down to the sub-ML level, and operates in the absence of either surfactants or reducing agents, ¹⁴ it is considerably more complex and more unwieldy than simple electrodeposition. The (i) need for conductive species present in solution, the (ii) lack of obvious scalability, coupled with the (iii) longer reaction times and (iv) careful experimentation necessary to achieve uniform, reliable, and precise shell thicknesses denote apparent disadvantages of this UPD/GD process. ^{14,19}

Lastly, the use of microwave irradiation has revealed much promise as an alternative, energyefficient means of chemical synthesis, especially of non-conductive materials. Microwaves possess wavelengths in the size range between a meter and a millimeter, and can be selectively absorbed by polar molecules. The rapid heating²⁰ common to microwave-assisted techniques therefore allows for faster reaction rates, implying overall shorter reaction times²¹ and reductions in energy consumption. These attributes, along with the capability of reproducibly achieving high yields under relatively mild reaction conditions,²² render microwave-assisted techniques as an arguably more 'sustainable' approach as compared with conventional heating methods.²³ In microwave-assisted syntheses, reaction variables, such as but not limited to power, frequency, precursor identity, the precursor concentration ratio, surfactant choice, the nature of the reducing agent, solvent selection, duration time, and reaction temperature, can be purposefully optimized to dictate the size, shape, and crystallinity of the desired nanostructures. Moreover, microwave treatments can allow for a more 'even' dispersal of heat throughout the sample as compared with conventional protocols. Disadvantages of this approach include the (i) possibility of a more polydisperse distribution of isolated product sizes and shapes, ²¹ the (ii) requirement of using a solvent with a sufficiently large dielectric constant to effectively absorb microwave energy, ²¹ in addition to a (iii) general lack of

mechanistic understanding of particle nucleation, growth kinetics, and compositional control under microwave irradiation conditions.²²

Each of these protocols can be viewed as complementary to each other in generating the desired core-shell architectures. None is necessarily 'better' than the others, but taken collectively, these strategies provide for a helpful toolkit with which to produce unique materials, whose overall characteristic attributes are often different from and potentially better than those of their individual constituent components. We proceed to take a closer look at each of these methodologies and their implications for both the resulting structures and their corresponding applications.

2.1 Electrodeposition.

Prior to our study, the fundamental issue of predictively tuning the thickness of silica on carbon nanotubes (CNTs) remained an unresolved issue.²⁴⁻²⁶ Previously published experimental protocols for silica deposition involved (i) the use of strongly acidic or basic conditions, (ii) excessive reaction times, and/or (iii) the formation of unwanted byproducts with (iv) often very little if any demonstrable control over the magnitude of the as-produced, external silica coating.

The importance of a protective coating of silica is that it can limit potential damage to the favorable mechanical and electronic properties of CNTs.²⁷ Specifically, the presence of a silica coating can minimize not only tube-tube contact and bundle formation but also tube oxidation, which is important to the use of appropriately functionalized CNTs as individualized gate dielectric materials within the context of field effect transistors.²⁸ In terms of additional benefits, first, a thin SiO₂ / SiO_x coating is optically transparent, and second, silica itself is biocompatible. Hence, the ability to reproducibly produce a thin, transparent, and biocompatible coating of silica onto underlying CNT surfaces has key implications for not only optics but also biomedical applications.

As such, we developed facile algorithms to reliably coat CNTs with various discrete thicknesses of silica using an electrochemical sol-gel process. In effect, we demonstrated the feasibility of two distinctive experimental protocols. In one procedure, a CNT mat itself was used as a working electrode for the direct deposition of silica. In the second complementary procedure, CNTs were initially dispersed in solution, after which silica was deposited onto these solubilized nanotubes in the presence of a Pt working electrode. The application of a negative potential led to silica condensation onto the underlying CNT surface. Indeed, we showed that by using two different and complementary procedures, CNTs could be coated with a uniform and consistent thickness of silica film by purposefully modulating (i) the magnitude of the potential of the working electrode, (ii) the concentration of the precursor sol solution, and (iii) the deposition time.

In essence, our electrochemical strategy was advantageous in several key aspects. First, the silica appeared to coat the CNTs in a non-covalent and hence, desirably non-destructive fashion through van der Waals interactions, as suggested by spectroscopy data, such that the attractive physical properties of the CNTs were conserved after the processing treatment. Second, the coating procedure itself was reasonably mild and sustainable to the extent that minimum amounts of the reactants were used under relatively gentle conditions that were neither overly acidic nor unduly basic. Third, the measured reaction time necessary to induce electrodeposition was relatively short, e.g. only 5 to 10 min, to complete the process. Fourth, all of the experiments were performed at room temperature under ambient conditions. Nevertheless, because the sol-gel process²⁹ yielded deposited films, whose resulting structure was determined by factors such as (i) the precursor size, structure, and reactivity, (ii) relative rates of condensation and evaporation, and (iii) liquid surface tension, not surprisingly, we noted that an increase in film thickness was marked by a corresponding rise in the surface roughness of the silica coating.

Based on AFM measurements, the actual thickness of the silica film could be calculated by subtracting the average height of the uncoated sections of the CNT bundles from that of the coated regions of CNT bundles within the same sample. Therefore, in terms of achieving meaningful structure-parameter correlations, the thickness of the silica films on the CNTs could be adjusted from \sim 4.4 \pm 1.3 nm to 26.6 \pm 6.8 nm by increasing the magnitude of the negative potential applied from \sim 500 mV to \sim 1000 mV with the silica depositing at a rate of 0.044 nm/mV (**Figure 2A**). Furthermore, the silica coating thickness increased from 3.4 \pm 1.2 nm to 31.5 \pm 7.2 nm in a linear manner as function of the tetramethoxysilane (TMOS) precursor concentration used; indeed, we were able to show an empirical relationship between silica thickness and reagent concentration with an apparent measurable shell growth of \sim 56.4 nm for every mM of precursor used (**Figure 2B**). Overall, these quantitative results highlighted the key advantages of our protocol, ⁴ relevant to the theme of this Account, namely our ability to carefully fine tune the outer silica film thickness onto underlying inner CNT surfaces through a reproducible, solution-derived electrodeposition process.

2.2. Electrospinning.

Our contribution to this body of work was to put forth a one-step coaxial electrospinning process³ (Figure 3A) for producing inorganic nanofibers comprising a well-defined core-shell structure coupled with a tunable internal morphology (e.g. evolving from hollow cavities to filled channels, depending on the synthesis parameters and electrospinning conditions used). Specifically, we were able to fabricate core-shell SnO₂/TiO₂ nanofibers in only one simple step. Within our home-built system, incorporating a dual spinneret with coaxial geometry, the core solution was fed into the inner spinneret, whereas the shell solution was flowed into the outer one. As such, coaxial fibers could be generated under high voltage conditions. The enhanced photocatalytic performance of our as-prepared tubular SnO₂/TiO₂ systems as compared with commercial TiO₂ control samples could be

ascribed to a number of reasons, including (i) an increase in charge-separation efficiency, (ii) the facilitation of efficient interparticle charge transfer; and (iii) the exposure of available reactive area for both photogenerated electrons and holes.

In line with the theme of this Account of introducing a degree of order and systematicity to a nanoscience-based synthesis protocol, we also analyzed various reaction parameters, such as Sn²⁺ precursor, applied voltage, and the feeding rate, in order to consider both their qualitative and quantitative effects upon the observed products.³ For example, by systematically increasing the concentration of the Sn²⁺ precursor from 1.6 mmol/mL, then to 2.2 mmol/mL and finally to 3.0 mmol/mL, respectively, the isolated morphology of electrospun fibers evolved from that of (i) a tubular coaxial structure to (ii) a peapod-like structure, and finally, onwards to (iii) a solid, filled core-shell structure (Figure 3B). It is worth noting that within these peapod structures, magnified high resolution TEM images of a representative interface between the TiO₂ and SnO₂ components indicated that the boundary between these two oxide constituent structures was characterized by particle grains measuring 10 to 20 nm in size, coupled with an evident spatial differentiation between the individual Sn and Ti signals, supporting the idea of the creation of two monocrystalline phases. The analogous cross-sectional TEM image of solid SnO₂/TiO₂ nanofibers suggested that the fibers consisted of a thick shell, comprised of loosely packed 20 nm-diameter nanoparticles (NPs), in conjunction with a denser circular, ~50 nm-diameter central core (Figure 3C).

Altering either the feeding rate or the magnitude of the applied voltage did not appear to have as much of an apparent effect upon the fiber morphology itself. That is, at a given feeding rate, the average diameter of fibers essentially remained constant within a relatively narrow range of 272 to 285 nm, whereas the inner diameter only slightly broadened from 104 to 122 nm, when the applied

voltage was decreased from 7 to 5 kV. However, the measured inner diameter of tubular SnO₂/TiO₂ nanofibers was significantly impacted by the inner tube feeding rate itself.

Specifically, when the inner feeding rate was systematically increased from ~0.03 mL/h, 0.10 mL/h, and finally to 0.15 mL/h, the diameter of the inner cavity correspondingly increased in magnitude from 60, 122, and ultimately to 164 nm, with the overall apparent fiber diameter similarly trending upwards from 236, 285, and finally to 301 nm, respectively (**Figure 3B**). By comparison, the inner core diameter of analogous solid SnO₂/TiO₂ nanofibers could be tuned in the range of 30 to 60 nm by correspondingly adjusting the inner feeding rate from 0.05 to 2 mL/h; within this same range of feeding rates, the dimensions of the fiber themselves rose from 194 to 345 nm.

2.3. Underpotential deposition (UPD) and galvanic displacement reactions.

As a potentially elegant structural solution to reducing overall precious metal content incorporated within functional catalysts, the use of core-shell architectures comprised of Pt monolayers (MLs) or skins for electrocatalysis has allowed for meaningful reductions in Pt utilization, because relatively scarce, expensive precious metals can be substituted with more abundant and less expensive metals.³⁰ That is, within the context of a 'M' (wherein 'M' = transition metal) core - Pt-based shell architecture, such a motif maximizes Pt use, minimizes Pt loading, and potentially enables every Pt atom to be catalytically accessible. Moreover, within a core-shell configuration, desirable synergistic interactions between the inner core and the outer shell, arising from a confluence of ligand and strain effects, can facilitate charge transfer and increase reaction kinetics, thereby leading to measurable enhancements in electrochemical activity and durability.³¹

In early studies within our group, we fabricated Pt-based core-shell NWs by depositing ML quantities of Pt onto our underlying core metal NW surfaces by customizing an under-potential deposition (UPD) / galvanostatic deposition (GD) protocol. ^{32,33} Experimentally, the Pt 'shells' were

created by first electrodepositing a conformal Cu monolayer with an initial UPD process, followed by subsequent displacement of the Cu ad-atoms with Pt via galvanic displacement. In principle, the exact spatial extent of the Pt ML coverage could be systematically tuned and appropriately varied by repeating, as necessary, the UPD/GD step, so as to yield a thicker, more uniform, contiguous, and homogeneous protective "Pt coat".

These established methods for core-shell motif synthesis clearly worked. As an example, we generated not only ultrathin 1-D Pd_{1-x}Cu_x alloys but also Pt-coated Pd_{1-x}Cu_x (i.e. Pt~Pd_{1-x}Cu_x) coreshell hierarchical nanostructures of arbitrary chemical compositions by initially utilizing a straightforward, surfactant-based, wet chemical synthesis followed by implementation of the UPD/GD process (Figure 4A).³⁴ In particular, as-prepared Pt~Pd_{1-x}Cu_x nanowires consistently outperformed not only commercial Pt NPs but also ultrathin Pt NWs by several fold orders of magnitude for both the methanol oxidation (MOR) and ethanol oxidation (EOR) reactions in alkaline media (Figure 4A). In a separate example, we demonstrated that the deposition of Pt onto template-derived, pure crystalline Ru NWs (Pt~Ru NWs) generated a unique hierarchical structure, wherein the immobilized Pt existed as discrete, "island-like" clusters on the surface (Figure 4B).³⁵ These Pt~Ru NWs not only gave rise to significantly improved activity metrics (i.e., double the peak current density along with a 100 mV lower onset potential) as compared with commercial Pt NP/C, but also evinced noteworthy durability, even after 2000 cycles of rigorous testing (Figure 4B).

In particular, our group sought to understand the physical and electronic structure of this Pt ML formation in more chemically and physically precise terms, so as to be able to more accurately explain the mechanistic rationale, underpinning these observations. Moreover, we had additional motivation in accounting for our data, because (i) our highest-performing NWs used as the core platform tended to possess predominantly ultrathin size dimensions (i.e., < 5 nm in average

diameter), and (ii) we had developed a modified, generalizable 'bulk' gram-scale process for these ultrathin NWs,³⁶ consisting of (a) a UV/ozone treatment followed by (b) CO stripping and (c) Pt deposition. Understanding the nature of the products created out of a sustainable, large-scale, nanochemistry-based synthesis protocol became a valuable objective.

As a test system for our studies,^{37,38} we had shown that (i) as-prepared Pd₉Au NWs evinced significantly enhanced oxygen reduction reaction (ORR) activity (0.40 mA/cm²) as compared with both elemental Pd NWs and NPs (Figure 5A), and that (ii) upon deposition of a Pt ML (Figure 5B), Pt~Pd_{1-x}Au_x NWs possessed notably higher and favorable surface area and mass-normalized activities of 0.98 mA/cm² and 2.54 A/mg_{Pt}, respectively (Figure 5C-D). However, the precise spatial localization of Pt, Au, and Pd elements within the core-shell motif itself remained a mystery. This issue was complicated by the fact that Pt and Au atoms could not be readily differentiated, based on an analysis of the energy dispersive X-ray analysis (EDS) spectra alone, due to the unfortunately close and overlapping signature bands associated with these individual metals.

We therefore sought to address these problems with a combined experimental and theoretical approach (Figure 6).² Using density functional theory (DFT), for Pt~Pd_{1-x}Au_x NWs incorporating various Pd-to-Au ratios, we simulated three possible geometric variations (Figure 6B) to generate a plausible picture, concerning the spatial elemental distribution of Au atoms within these ultrathin NWs. Scenario 1 concentrated all of the Au atoms within the core itself. In Scenario 2, a percentage of the Au atoms was segregated at the edge of the Pt shell. Finally, in Scenario 3, all of the Au atoms were confined within the outer Pt shell. The full localization of Au in the shell could both stabilize the NWs and boost NW rigidity, thereby not only preventing structural distortion effects upon oxygen adsorption but also weakening the oxygen binding energy, a proxy for experimental ORR

kinetics and activities. In essence, the model proposing complete Au surface segregation yielded a similar theoretical ORR activity trend to that of the actual experiment (**Figure 6A**).

Because extended X-ray absorption fine structure (EXAFS) spectroscopy can be used to evaluate the local atomic environment within both bulk and nanomaterial systems, we conducted a series of time-dependent *in situ* EXAFS experiments to enable us to probe the consequences of the ORR reaction on the possible restructuring of our core-shell Pt \sim PdAu nanowires. We hypothesized that the surface catalysis of O₂ species accounted for our observed structural modification. From a combined analysis of the acquired Pt L_3 and Au L_3 edges, the only consistent picture that reconciled both data sets was one in which the Au atoms were well dispersed with the Pt layer itself, thereby creating a PtAu-shell / Pd-core structure.

The combination of complementary and corroborating results from (a) in situ X-ray absorption spectroscopy (namely Pt and Au L edge data), (b) DFT calculations, and (c) electrochemical data within a comprehensive, holistic analysis led to an improved understanding of the physico-chemical properties of these NWs.² We concluded that the catalytically active structure of our ternary nanowires consisted of a PtAu~Pd motif, defined by an outer PtAu binary shell coupled with a pure inner Pd core. The plausible origin of the observed Au surface segregation could likely be attributed to the actual synthesis conditions, i.e. the external potential used (i.e., within the range of 0.5-0.8 V) during the Cu UPD process itself to create the alloyed NW motif in the first place, implying that the 'reconstruction' process occurred primarily upon polarization.

2.4. Microwave-Assisted Chemistry.

In a recent study, using microwave-assisted chemistry,¹ we synthesized and probed a coreshell structure, characterized by an inner Cu NW surrounded by an outer TiO₂ layer. This core-shell motif not only maximized the use of an inexpensive, abundant, but still catalytically active Cu core

but also enabled the ability to customize the size of the TiO₂ shell so as to optimize catalytic reactivity. Whereas prior microwave methods³⁹ had used inherently hazardous Ti precursors, in terms of novelty, our approach was different and distinctive for several crucial reasons. *First*, we modified the microwave-based synthesis protocol to incorporate a safer precursor molecule, i.e. titanium butoxide, TBOT, within the context of an aqueous, surfactant-free methodology, so as to maximize catalytic performance by minimizing the presence of any residual impurities. *Second*, we systematically adjusted reaction variables, such as precursor amounts, the method of precursor addition, and reaction time, to controllably tune shell thickness and to tailor shell uniformity around the underlying Cu NW core without unnecessarily damaging it. This strategy led to a similar outcome we had sought in the context of the quantitative silica functionalization of CNTs.

In effect,¹ the synthesis of Cu@TiO₂ core@shell catalytic NW structures was thoroughly investigated using a microwave-assisted method through the tuning of experimental parameters such as (i) the controlled variation in molar ratios, (ii) the use of different Ti precursors, (iii) the method of addition of the precursors themselves, and (iv) the irradiation time. Homogeneous coatings were generated using Cu: Ti molar ratios of 1: 2, 1: 1, 2: 1, and 4: 1, respectively (Figure 7A). The TiO₂ shell dimension was primarily impacted by changes in the corresponding quantity of precursor used, although the dependence was decidedly non-linear. Nonetheless, by systematically decreasing the amount of TBOT from 0.1 mL to 0.025 mL, the shell size correspondingly reduced in magnitude from ~37 to 10.7 nm. Moreover, we observed a slight downward trend and a corresponding lattice contraction with decreasing titania shell size, perhaps due to a compression-like strain effect induced upon the external TiO₂ ML-like shell as a result of the underlying Cu(110) core.⁴⁰

Performance-wise, our Cu@TiO₂ core-shell NW samples, regardless of the pre-treatment conditions, yielded as much as 20 times higher catalytic activity as compared with standard Cu NW

controls (Figure 7D). These data underscore the importance of the metal-semiconducting Cu/TiO₂ interface in terms of promoting CO₂ hydrogenation. We also systematically tracked the structural and chemical evolution of our catalysts, both before and after CO₂ reduction. After the reaction process, the 1: 2 Cu: Ti molar ratio sample in particular was characterized by the appearance of appreciably greater amounts of clusters of well-defined, catalytically active Cu NPs, atop the underlying core@shell motif (Figure 7B). This morphological anomaly, likely originating from the active diffusion of Cu species from the central core to the outer surface, could account for the greater CO₂ reduction activity observed. It is worth noting that the structural integrity of the core@shell wire motif was essentially conserved (Figure 7C) even after this relatively high-temperature, potentially destructive reaction process, thereby reinforcing the inherent thermal stability and physical robustness of our as-prepared hierarchical structures.

3. Summary and Future Directions.

In this Account, we have outlined the viability, versatility, and diversity of possible solutions to generating different, intrinsically tunable core-shell motif structures, highlighting that there are many legitimate approaches (Table 1) to trying to address this challenging synthetic problem. Each of the four methods we have discussed herein offers the ability to provide reasonable (often quantitative) control over shell morphology and dimensionality through the optimization of experimental parameters. For instance, the shell precursor quantity dictated the resulting shell sizes, when using electrodeposition, electrospinning, and microwave-assisted methods, whereas for the UPD/GD protocol, the precise extent of ML and sub-ML formation could be adjusted by the number of times the UPD/GD step had been repeated. Furthermore, the homogeneity of the outer shell could be impacted primarily by factors, such as the magnitude of the applied voltage in the cases of electrodeposition and electrospinning. By contrast, precursor type, method of shell precursor

addition, and irradiation time were more significant determinants of shell uniformity in the case of microwave-based techniques. The inherent flexibility and demonstrated efficacy of this synthetic toolkit is particularly important, considering that well-defined core-shell materials have found broad use in a wide variety of key applications, spanning energy, ¹⁴ biomedicine, ⁴¹ sensing, ²¹ in addition to electrochemical, thermochemical, and photochemical catalysis. ^{1,21,22}

Nevertheless, daunting difficulties remain. One key limitation is that whereas promising methods, such as ambient solution-phase processes, ⁴² have been developed for the synthesis of a variety of metal-based core—shell NWs, there are no comparably reliable and sustainable protocols, that will consistently yield a sharp, atomically precise interface (without mixing) between core and shell materials of *any* arbitrary composition and size. As an example, electrochemical methods work best with conductive systems but are often far less effective with either semiconducting or insulating species. Because we have centered our discussion on 1D NWs herein, a related concern is a lack of generalizable protocols that will enable the quantifiable manipulation of core-shell systems, based on a dissimilar dimensionality, such as either 0D NPs or more complicated structures. As examples, there are relatively few reports, centered on creating viable core@shell architectures, incorporating either 2D nanosheets or complex 3D hierarchical motifs.⁴³

Moreover, from a theoretical perspective, reports have surfaced on the influence and effects of shell strain and geometric parameters (such as shell thickness) on the valence band structure and transport properties of not only semiconducting III-V systems⁴⁴ but also related alloyed materials.⁴⁵ The dependence of the effective gap on variables, such as the core radius and NW shell identity, has been postulated within semiconducting core-shell NWs.⁴⁶ As such, being able to readily relate geometric and material properties, including not only mismatch strain between core and shell⁴⁷ but also shell thickness,⁴⁸ with measurable observables, such as optical photoluminescence, elasticity,⁴⁹

magnetic behavior,^{50,51} and electron mobility,⁵² would be intrinsically useful in acquiring consequential structure-property correlations. Yet, at a basic level, reports on the facile, large-scale synthetic protocols that can fabricate homogeneous, monodisperse core-shell structures at gram and kilogram levels are few and far between, meaning that a thorough and comprehensive characterization of these materials is limited by the simple fact of not having enough quantities of sample to work with. As a result, theoretical predictions cannot be easily verified.

Furthermore, it is still experimentally challenging to 'routinely' track the spatial and temporal evolution of the physical structure and the chemical composition of (a) the core, (b) the shell, and (c) the resulting interface between them, while analyzing the functional behavior (e.g., catalytic) of core-shell structures under realistic operando conditions, using dynamic in situ characterization techniques. Our ORR studies with Pt~PdAu core-shell NWs coupled with our CO₂ hydrogenation work on Cu@TiO₂ core-shell NWs highlighted local and subtle changes in chemical composition and physical structure that often occur during a reaction process with potentially unforeseen consequences for the observed reactivity. As such, variations in atomic packing, degree of chemical functionalization, defect content, and/or extent of crystallinity can impact upon observed properties with considerable implications for performance, mechanism, and durability.

Many of these issues can be addressed to some extent by achieving a well-defined atomistic and molecular understanding of how core-shell motifs precisely nucleate and grow under diverse solution-based reaction conditions. However, to do so, transformative advances will need to be made to overcome the series of experimental and theoretical obstacles we have identified herein.

4. Acknowledgements.

This material is based on work supported by the U.S. National Science Foundation under Grant No. CHE-1807640.

5. Biographical Information:

Kenna L. Salvatore received her B.Sc. degree in Chemistry at James Madison University. She is currently pursuing her Ph.D. studies in the Wong group at Stony Brook University. Her interests lie in probing the synthesis and corresponding applications of nanomaterials for energy. Stanislaus S. Wong obtained his B.Sc. (Honours) degree at McGill University in addition to his A.M. and Ph.D. degrees at Harvard University. After postdoctoral studies conducted at Columbia University, he was hired by Stony Brook University as an Assistant Professor with a joint appointment at Brookhaven National Laboratory. He is currently a SUNY Distinguished Professor of Chemistry at Stony Brook University. He and his group have worked on developing viable sustainable strategies for generating novel nanomaterials of relevance not only for batteries, fuel cells, and solar cells, but also for nanomedicine and theranostics.

References

- (1) Salvatore, K. L.; Deng, K.; Yue, S.; McGuire, S. C.; Rodriguez, J. A.; Wong, S. S. Optimized Microwave-based Synthesis of Thermally-Stable Inverse Catalytic Core-Shell Motifs for CO₂ Hydrogenation. *ACS Applied Materials and Interfaces* **2020**, *12*, 32591-32603.
- (2) Liu, H.; An, W.; Li, Y.; Frenkel, A. I.; Sasaki, K.; Koenigsmann, C.; Su, D.; Anderson, R. M.; Crooks, R. M.; Adzic, R. R.; Liu, P.; Wong, S. S. In Situ Probing of the Active Site Geometry of Ultrathin Nanowires for the Oxygen Reduction Reaction. *J. Am. Chem. Soc.* **2015**, *137*, 12597-12609.
- (3) Peng, X.; Santulli, A. C.; Sutter, E.; Wong, S. S. Fabrication and Enhanced Photocatalytic Activity of Inorganic Core-shell Nanofibers Produced by Coaxial Electrospinning. *Chemical Science* **2012**, *3*, 1262 1272.
- (4) Kanungo, M.; Isaacs, H. S.; Wong, S. S. Quantitative Control over Electrodeposition of Silica films onto Single-Walled Carbon Nanotube Surfaces. *J. Phys. Chem. C* **2017**, *111*, 17730-17742.
- (5) Reich, D. H.; Tanase, M.; Hultgren, A.; Bauer, L. A.; Chen, C. S.; Meyer, G. J. Biological applications of multifunctional magnetic nanowires. *J. Appl. Phys.* **2003**, *93*, 7275-7280.
- (6) Sarkar, J.; Khan, G. G.; Basumallick, A. Nanowires: properties, applications and synthesis via porous anodic aluminium oxide template. *Bull. Mater. Sci.* **2007**, *30*, 271-290.
- (7) Koenigsmann, C.; Tan, Z.; Peng, H.; Sutter, E.; Jacobskind, J.; Wong, S. S. Multifunctional Nanochemistry: Ambient, Electroless, Template-Based Synthesis and Characterization of Segmented Bimetallic Pd/Au and Pd/Pt Nanowires as High-Performance Electrocatalysts and Nanomotors. *Isr. J. Chem.* **2012**, *52*, 1090 1103.
- (8) Kuchibhatla, S.; Karakoti, A. S.; Bera, D.; Seal, S. One dimensional nanostructured materials. *Prog. Mater Sci.* **2007**, *52*, 699-913.
- (9) Lieber, C. M. One-Dimensional Nanostructures: Chemistry, Physics & Applications. *Solid State Commun.* **1998**, *107*, 607-616.
- (10) Weber, J.; Singhal, R.; Zekri, S.; Kumar, A. One-dimensional nanostructures: fabrication, characterisation and applications. *Int. Mater. Rev.* **2008**, *53*, 235-255.
- (11) Zhang, X. N.; Li, C. R.; Zhang, Z. Controlling the growth direction of one-dimensional ZnO nanostructures by changing the oxygen content in the reaction atmosphere. *Appl. Phys. A: Mater. Sci. Process.* **2006**, *82*, 33-37.
- (12) Meng, X. Q.; Peng, H.; Gai, Y. Q.; Li, J. Influence of ZnS and MgO Shell on the Photoluminescence Properties of ZnO Core/Shell Nanowires. *The Journal of Physical Chemistry C* **2009**, *114*, 1467-1471.
- (13) Park, J. Y.; Choi, S. W.; Lee, J. W.; Lee, C.; Kim, S. S. Synthesis and Gas Sensing Properties of TiO₂-ZnO Core-Shell Nanofibers. *J. Am. Ceram. Soc.* **2009**, *92*, 2551-2554.
- (14) Wang, R.; Wang, H.; Luo, F.; Liao, S. Core–Shell-Structured Low-Platinum Electrocatalysts for Fuel Cell Applications. *Electrochemical Energy Reviews* **2018**, *1*, 324-387.
- (15) Ramakrishna, S.; Jose, R.; Archana, P. S.; Nair, A. S.; Balamurugan, R.; Venugopal, J.; Teo, W. E. Science and engineering of electrospun nanofibers for advances in clean energy, water filtration, and regenerative medicine. *J. Mater. Sci.* **2010**, *45*, 6283-6312.

- (16) Yoon, J.; Yang, H.-S.; Lee, B.-S.; Yu, W.-R. Recent Progress in Coaxial Electrospinning: New Parameters, Various Structures, and Wide Applications. *Adv. Mater.* **2018**, *30*, 1704765.
- (17) Chen, J. S.; Chen, Z.; Chen, R. Y.; Zheng, X.; Chen, X. Preparation and photocatalytic properties of NiO-TiO₂ coaxial nanofibers. *Acta Materiae Compositae Sinica* **2011**, *28*, 36-41.
- (18) Szilágyi, I. M.; Nagy, D. Review on one-dimensional nanostructures prepared by electrospinning and atomic layer deposition. *Journal of Physics: Conference Series* **2014**, *559*, 012010.
- (19) Wang, X.; He, B.; Hu, Z.; Zeng, Z.; Han, S. Current advances in precious metal core–shell catalyst design. *Science and Technology of Advanced Materials* **2014**, *15*, 043502.
- (20) Liao, X.-H.; Chen, N.-Y.; Xu, S.; Yang, S.-B.; Zhu, J.-J. A microwave assisted heating method for the preparation of copper sulfide nanorods. *J. Cryst. Growth* **2003**, *252*, 593-598.
- (21) Mirzaei, A.; Neri, G. Microwave-assisted synthesis of metal oxide nanostructures for gas sensing application: A review. *Sensors and Actuators B: Chemical* **2016**, *237*, 749-775.
- (22) Kumar, A.; Kuang, Y.; Liang, Z.; Sun, X. Microwave chemistry, recent advancements, and eco-friendly microwave-assisted synthesis of nanoarchitectures and their applications: a review. *Materials Today Nano* **2020**, *11*, 100076.
- (23) Polshettiwar, V.; Nadagouda, M. N.; Varma, R. S. Microwave-assisted chemistry. A rapid and sustainable route to synthesis of organics and nanomaterials. *Aust. J. Chem.* **2009**, *62*, 16-26.
- (24) Bottini, M.; Tautz, L.; Huynh, H.; Monosov, E.; Bottini, N.; Dawson, M. I.; Bellucci, S.; Mustelin, T. Covalent decoration of multi-walled carbon nanotubes with silica nanoparticles. *Chem. Commun.* **2005**, *6*, 758-760.
- (25) Vast, L.; Philippin, G.; Destree, A.; Moreau, N.; Fonseca, A.; Nagy, J. B.; Delhalle, J.; Mekhalif, Z. Chemical functionalization by fluorinated trichlorosilane of multiwalled carbon nanotubes. *Nanotechnology* **2004**, *15*, 781-785.
- (26) Fan, W.; Gao, L. Silica nanobead-decorated multi-walled carbon nanotubes by vapor-phase method. *Chem. Lett.* **2005**, *34*, 954-955.
- (27) Dresselhaus, M. S.; Dresselhaus, G.; Avouris, P.: Carbon Nanotubes: Synthesis, Structure, Properties, and Applications; Springer Verlag: Berlin, 2001.
- (28) Wind, S.; Appenzeller, J.; Martel, R.; Derycke, V.; Avouris, P. Vertical Scaling of Single-Wall Carbon Nanotube Transistors Using Top Gate Electrodes. *Appl. Phys. Lett* **2002**, *80*, 3817-3819.
- (29) Brinker, C. J.; Frye, G. C.; Hurd, A. J.; Ashley, C. S. Fundamentals of Sol-Gel Dip Coating. *Thin Solid Films* **1991**, *201*, 97-108.
- (30) Adzic, R.; Zhang, J.; Sasaki, K.; Vukmirovic, M.; Shao, M.; Wang, J.; Nilekar, A.; Mavrikakis, M.; Valerio, J.; Uribe, F. Platinum Monolayer Fuel Cell Electrocatalysts. *Top. Catal.* **2007**, *46*, 249-262.
- (31) Wang, X.; Orikasa, Y.; Takesue, Y.; Inoue, H.; Nakamura, M.; Minato, T.; Hoshi, N.; Uchimoto, Y. Quantitating the lattice strain dependence of monolayer Pt shell activity toward oxygen reduction. *J. Am. Chem. Soc.* **2013**, *135*, 5938-5941.
- (32) Zhang, J.; Sasaki, K.; Sutter, E.; Adzic, R. R. Stabilization of Platinum Oxygen-Reduction Electrocatalysts Using Gold Clusters. *Science* **2007**, *315*, 220-222.

- (33) Vukmirovic, M. B.; Bliznakov, S. T.; Sasaki, K.; Wang, J. X.; Adzic, R. R. Electrodeposition of Metals in Catalyst Synthesis: The Case of Platinum Monolayer Electrocatalysts. *Electrochem. Soc. Interface* **2011**, *20*, 33-40.
- (34) Liu, H.; Adzic, R. R.; Wong, S. S. Multi-functional ultrathin Pd_xCu_{1-x} and Pt~Pd_xCu_{1-x} one-dimensional nanowire motifs for various small molecule oxidation reactions. *ACS Appl. Mater. Interf.* **2015**, *7*, 26145–26157.
- (35) Koenigsmann, C.; Semple, D. B.; Sutter, E.; Tobierre, S. E.; Wong, S. S. An Ambient Synthesis of High-Quality Ru Nanowires and the Morphology-Dependent Electrocatalytic Performance of Pt-decorated Ruthenium Nanowires and Nanoparticles in the Methanol Oxidation Reaction. *ACS Appl. Mater. Interf.* **2013**, *5*, 5518-5530
- (36) Shao, M. H.; Huang, T.; Liu, P.; Zhang, J.; Sasaki, K.; Vukmirovic, M. B.; Adzic, R. R. Palladium monolayer and palladium alloy electrocatalysts for oxygen reduction. *Langmuir* **2006**, *22*, 10409-10415.
- (37) Koenigsmann, C.; Sutter, E.; Adzic, R. R.; Wong, S. S. Size- and Composition-Dependent Enhancement of Electrocatalytic Oxygen Reduction Performance in Ultrathin Palladium–Gold (Pd_{1-x}Au_x) Nanowires. *J. Phys. Chem. C* **2012**, *116*, 15297-15306.
- (38) Koenigsmann, C.; Scofield, M. E.; Liu, H.; Wong, S. S. Designing Enhanced One-Dimensional Electrocatalysts for the Oxygen Reduction Reaction: Probing Size- and Composition-Dependent Electrocatalytic Behavior in Noble Metal Nanowires. *J. Phys. Chem. Lett.* **2012**, *3*, 3385-3398.
- (39) Liu, D.; Wu, B.; Mubeen, S.; Ding, K.; Zeng, H.; Chuong, T. T.; Moskovits, M.; Stucky, G. D. Microwave-Assisted Synthesis of Ultrastable Cu@TiO₂ Core-Shell Nanowires with Tunable Diameters via a Redox-Hydrolysis Synergetic Process. *ChemNanoMat* **2018**, *4*, 914-918.
- (40) Scofield, M. E.; Koenigsmann, C.; Bobb-Semple, D.; Tao, J.; Tong, X.; Wang, L.; Lewis, C. S.; Vukmirovic, M. B.; Zhu, Y.; Adzic, R. R.; Wong, S. S. Correlating the Chemical Composition and Size of Various Metal Oxide Substrates with the Catalytic Activity and Stability of As-Deposited Pt Nanoparticles for the Methanol Oxidation Reaction. *Catal. Sci.* **2016**, *6*, 2435-2450.
- (41) Zhang, Z.; Ji, D.; He, H.; Ramakrishna, S. Electrospun ultrafine fibers for advanced face masks. *Materials Science and Engineering: R: Reports* **2021**, *143*, 100594.
- (42) Stewart, I. E.; Shengrong, Y.; Zuofeng, C.; Flowers, P. F.; Wiley, B. J. Synthesis of Cu–Ag, Cu–Au, and Cu–Pt Core–Shell Nanowires and Their Use in Transparent Conducting Films. *Chem. Mater.* **2015**, *27*, 7788--7794.
- (43) Lu, W.; Guo, X.; Luo, Y.; Li, Q.; Zhu, R.; Pang, H. Core-shell materials for advanced batteries. *Chem. Eng. J.* **2019**, *355*, 208-237.
- (44) Palutkiewicz, T.; Wołoszyn, M.; Wójcik, P.; Adamowski, J.; Spisak, B. J. Influence of Geometrical Parameters on the Transport Characteristics of Gated Core-Multishell Nanowires. *Acta Phys. Pol., A* **2016**, *129*, A-111 A-113.
- (45) Xu, H.; Liu, X.; Du, G.; Zhao, Y.; He, Y.; Fan, C.; Han, R.; Kang, J. Effects of Shell Strain on Valence Band Structure and Transport Properties of Ge/Si_{1-x}Ge_x Core–Shell Nanowire. *Japanese Journal of Applied Physics* **2015**, *49*, 04DN01 / 01-05.
- (46) Luo, N.; Huang, G.-Y.; Liao, G.; Ye, L.-H.; Xu, H. Q. Band-inverted gaps in InAs/GaSb and GaSb/InAs core-shell nanowires. *Sci. Rep.* **2016**, *6*, 38698 / 38691-38611.

- (47) Skold, N.; Karlsson, L. S.; Larsson, M. W.; Pistol, M.-E.; Seifert, W.; Tragardh, J.; Samuelson, L. Growth and optical properties of strained GaAs-Ga_xIn_{1-x}P core-shell nanowires. *Nano Lett.* **2005**, *5*, 1943-1947.
- (48) Guo, J.-Y.; Zhang, Y.-W.; Shenoy, V. B. Morphological Evolution and Ordered Quantum Structure Formation in Heteroepitaxial Core-Shell Nanowires. *ACS Nano* **2010**, *4*, 4455–4462.
- (49) Cao, F.; Li, L.; Zheng, H.; Wen, G.; Zhao, L.; Liu, H.; Jia, S.; Wang, Z.; Hu, Y.; Gu, H.; Wang, J. Controllable Elasticity Storage and Release in CuO-Pt Core-Shell Nanowires. *ChemNanoMat* **2018**, *4*, 1140-1144.
- (50) Guo, H.; Jin, J.; Chen, Y.; Liu, X.; Zeng, D.; Wang, L.; Peng, D.-L. Controllable synthesis of Cu–Ni core–shell nanoparticles and nanowires with tunable magnetic properties. *Chem. Commun.* **2016**, *52*, 6918-6921.
- (51) Irfan, M.; Wang, C. J.; Khan, U.; Li, W. J.; Zhang, X. M.; Kong, W. J.; Liu, P.; Wan, C. H.; Liu, Y. W.; Han, X. F. Controllable synthesis of ferromagnetic–antiferromagnetic core–shell NWs with tunable magnetic properties. *Nanoscale* **2017**, *9*, 5694-5700.
- (52) Jiang, X.; Xiong, Q.; S.Nam; Qian, F.; Li, Y.; Lieber, C. M. InAs/InP radial nnanowire heterostructure as high electron mobility devices. *Nano Lett.* **2007**, *7*, 3214-3218.
- (53) Jiang, H. L.; Hu, Y. Q.; Li, Y.; Zhao, P. C.; Zhu, K. J.; Chen, W. L. A facile technique to prepare biodegradable coaxial electrospun nanofibers for controlled release of bioactive agents. *J. Controlled Release* **2005**, *108*, 237-243.
- (54) Yu, Y.; Gu, L.; Zhu, C. B.; van Aken, P. A.; Maier, J. Tin Nanoparticles Encapsulated in Porous Multichannel Carbon Microtubes: Preparation by Single-Nozzle Electrospinning and Application as Anode Material for High-Performance Li-Based Batteries. *Journal of the American Chemical Society* **2009**, *131*, 15984-15985.
- (55) Oezaslan, M.; Hasché, F.; Strasser, P. Pt-Based Core—Shell Catalyst Architectures for Oxygen Fuel Cell Electrodes. *The Journal of Physical Chemistry Letters* **2013**, *4*, 3273-3291.

Figure Captions

Figure 1. Scheme highlighting viable routes towards precise, quantifiable structural control of 1D core/shell NW motifs along with potential applications.

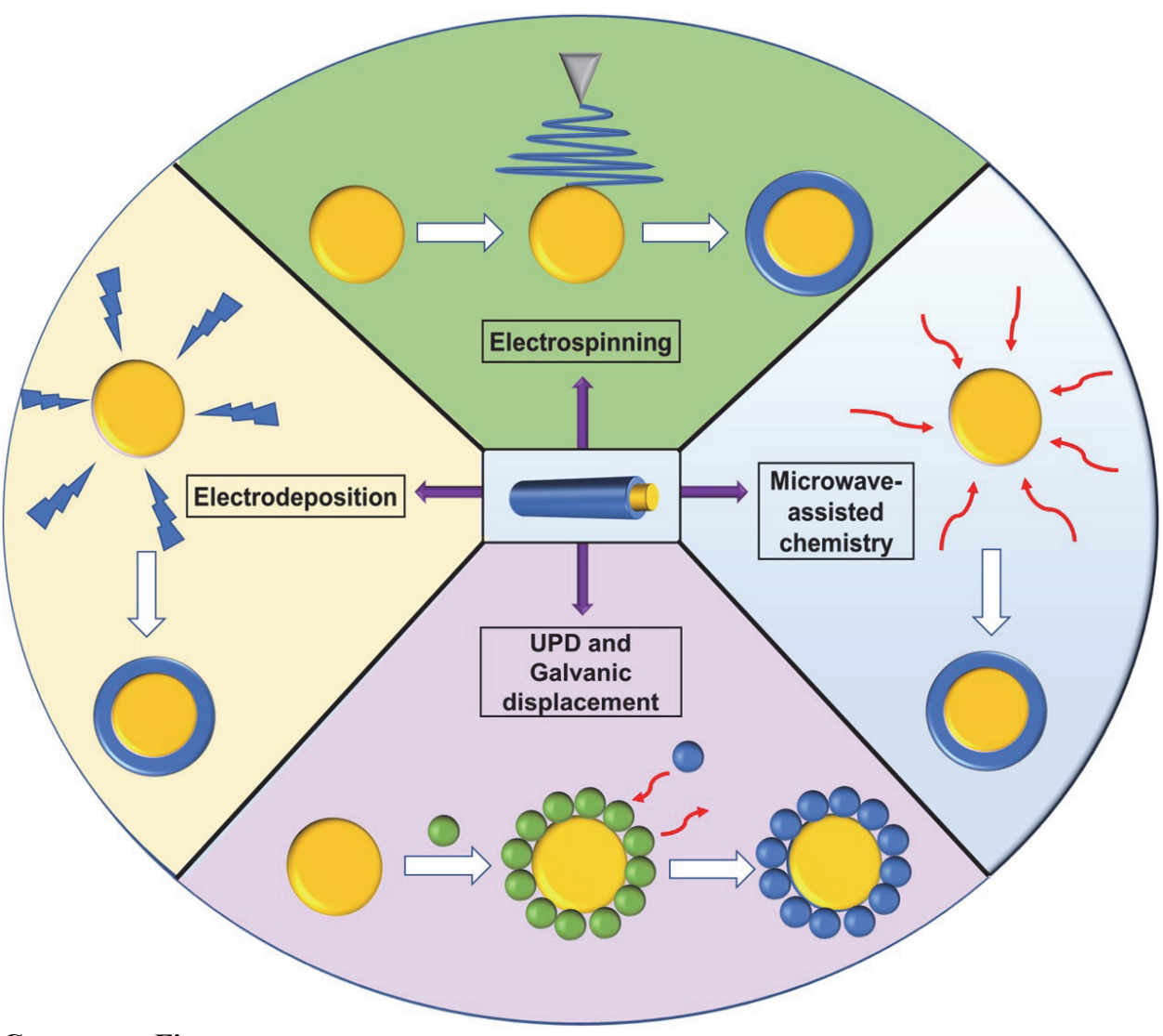
Figure 2A. Electrodeposition. (a-c). AFM height images of silica-coated CNTs synthesized by electrochemical silylation using a CNT mat electrode at -500, -700, and -1000 mV, respectively. Plots of the (d) heights and (e) film thicknesses of silica-coated CNTs vs. applied potential at various open circuit potential readings. Figure 2B. (a-c) AFM height images of silica-coated CNTs synthesized by electrochemical deposition onto CNTs dispersed in solution at potentials of -800, -900, and -1000 mV, respectively. (d-e). AFM heights and thicknesses of electrodeposited silica films at various negative applied potentials. (f-g). Increase in AFM heights and thicknesses of silica-coated CNTs probed as a function of silane concentration used. Letters U and C denote the relatively uncoated and correspondingly more heavily coated parts of the CNT bundles, respectively. Reproduced with permission from Ref. 4. Copyright 2017 American Chemical Society.

Figure 3A. Electrospinning. (left) Experimental set-up associated with co-axial electrospinning to generate tubular SnO₂/TiO₂ coaxial electrospun fibers. (right) Energy band diagram of SnO₂ and TiO₂ illustrates charge separation at the oxide interface and subsequent photocatalytic reaction. Figure 3B. By increasing the Sn precursor concentration, the morphology of asprepared SnO₂/TiO₂ electrospun fibers evolves (left to right) from a tubular coaxial structure to a peapod-like structure, and finally, onwards to a solid, filled core–shell structure. (a-c) Crosssectional TEM image of SnO₂/TiO₂ core-shell nanofibers. Figure 3C. (a-b) HRTEM images of peapod-like SnO₂/TiO₂ core shell nanofiber along with accompanying (c-d) SAED, (e) zoomed-

in magnification, and **(f)** EDS mapping results. Reproduced with permission from Ref. 3. Copyright 2012 Royal Society of Chemistry.

Figure 4A. UPD & Galvanic Displacement Processes. (left) (left) Representative TEM images for (A) Pd NWs, (D) Pd₉Cu NWs, (G) Pd₈Cu₂ NWs, and (J) Pd₇Cu₃ NWs, respectively. (right) EOR activity values for commercial Pt NPs, ultrathin Pt NWs, Pt~Pd NWs, Pt~Pd₉Cu NWs, Pt~Pd₈Cu₂ NWs, and Pt~Pd₇Cu₃ NWs, respectively. Figure panels reproduced with permission from reference 64. Figure 4B. Characterization of Pt-modified Ru NWs after one UPD/GD cycle, including relevant (A) TEM, (B) HAADF, and (C) spatially resolved EDAX mapping data. (right) Specific activities of the various electrocatalysts, including those of commercial Pt NP/C, alloy-type PtRu NP/C, optimized Pt~Ru NP/C, and PtRu NWs, measured at 0.65 V. Reproduced with permission from Ref. 43. Copyright 2013 American Chemical Society. Figure 5A. Ultrathin Pd_{1-x}Au_x NWs supported on Vulcan XC-72R carbon support, as ORR catalysts. Representative data include associated (A) TEM, (inset to A) HRTEM, (B) SAED pattern, (C) HAADF, and (D) EDAX spectra. Figure 5B. Schematic of process used to coat core Pd_{1-x}Au_x NWs using an initial UPD step involving Cu atoms followed by their galvanic displacement with Pt to yield an external Pt ML shell. Figure 5C. TEM results of as-synthesized Pt~Pd₉Au ultrathin NWs. (A) Bright-field imaging, (B) HAADF, (C) high-resolution STEM imaging, (D) cross-sectional EELS analysis. Figure 5D. Experimentally determined kinetic currents at 0.9 V normalized to the measured surface area and the platinum mass are shown for a series of Pt~Pd_{1-x}Au_x NW/C and commercial Pt NP/C, respectively. Reproduced with permission from Ref. 2. and Ref. 44. Copyright 2015 and 2012 respectively, American Chemical Society. Figure 6A. Comparing Theoretical and Experimental Results. (A) Theoretical estimated surface area activity (black) and mass activity (red) values for different chemical compositions in a range of Pd_(1-x)Pt_z@Au_xPt_(1-z) NWs, specifically on the *fcc* 3-fold sites. (B) Corresponding experimental results of ORR activities for a series of as-prepared Pt~Pd_{1-x}Au_x nanowires. **Figure 6B.** Hexagonal 2.2 nm-diameter [(111)4,(200)₂] nanowire models with various Au distributions. (a) Pd₉Au@Pt NWs, (b) Pd₈Au₂@Pt NWs, and (c) Pd₇Au₃@Pt NWs. Upper panel: (i) Pd_(1-x)Au_x@Pt NWs. Middle panel: (ii) Pd_(1-x)Au_(x-y)Pt_z@Au_yPt_(1-z) NWs. Lower panel: (iii) Pd_(1-x)Pt_z@Au_xPt_(1-z) NWs. Reproduced with permission from Ref. 2. Copyright 2015 American Chemical Society.

Figure 7A. Microwave-assisted Chemistry. Correlating the magnitude of the titania shell size (error bars included) with the initial Ti precursor amounts used, as derived from HRTEM images. Figure 7B. *Prior* to the CO₂ hydrogenation reaction. (A, B) TEM images, (C) high-resolution STEM image, and (D–G) HRTEM–EDS mapping of Cu@TiO₂ core@shell motifs, characterized by a 1:2 Cu/Ti molar ratio, after heat treatment but in the absence of any N₂ annealing. Figure 7C. *After* the CO₂ hydrogenation reaction. (A, B) TEM images, (C) high-resolution STEM image, and (D–G) HRTEM–EDS mapping of Cu@TiO₂ core@shell motifs, characterized by a 1:2 Cu/Ti molar ratio, after heat treatment but in the absence of any N₂ annealing. Figure 7D. Normalized CO₂ hydrogenation activity [in μmol/(gcus)] for Cu@TiO₂ samples in the absence of any N₂ annealing along with data for the corresponding Cu NW controls. Reproduced with permission from Ref. 1. Copyright 2020 American Chemical Society.



Conspectus Figure.

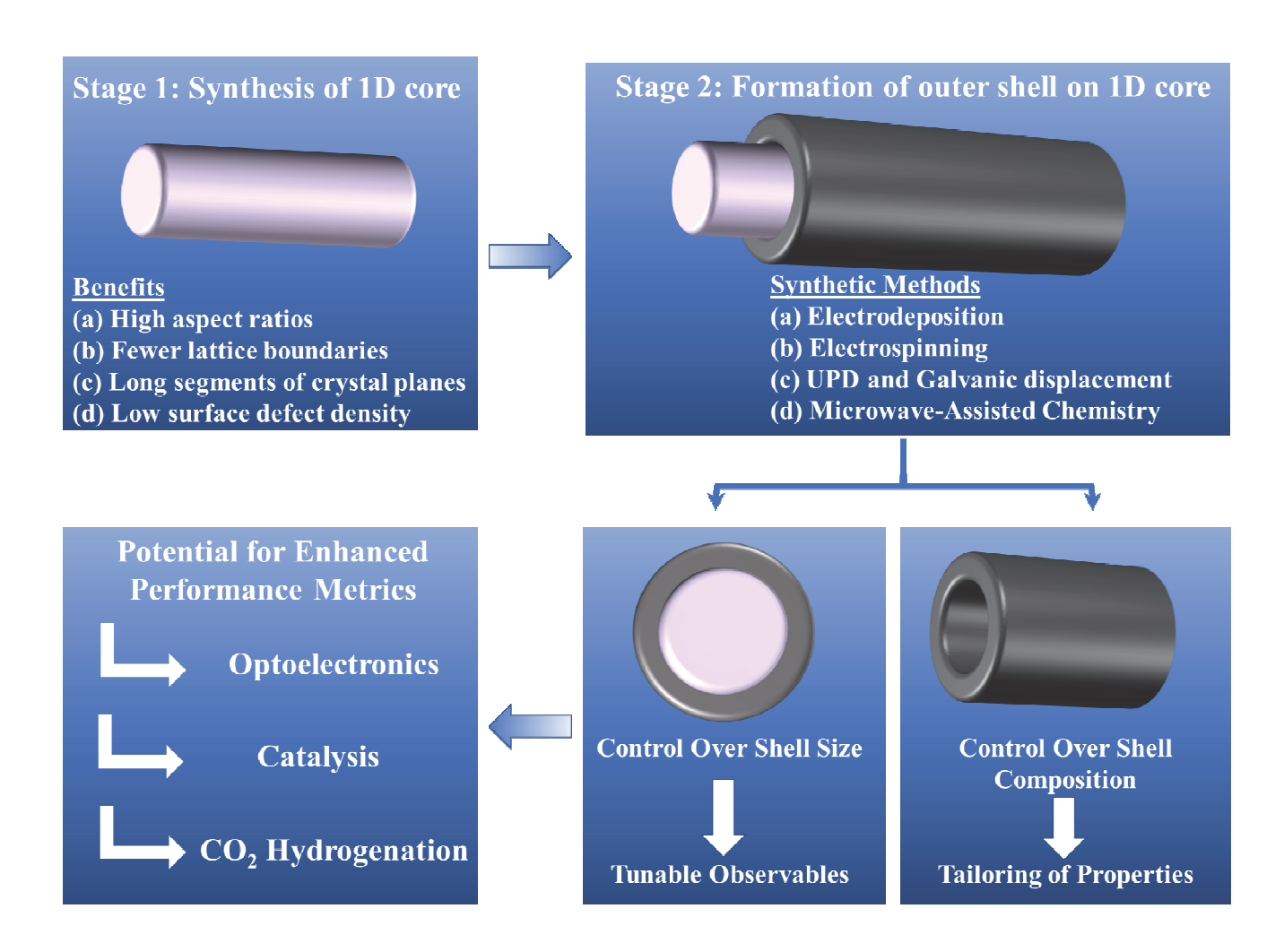


Figure 1.

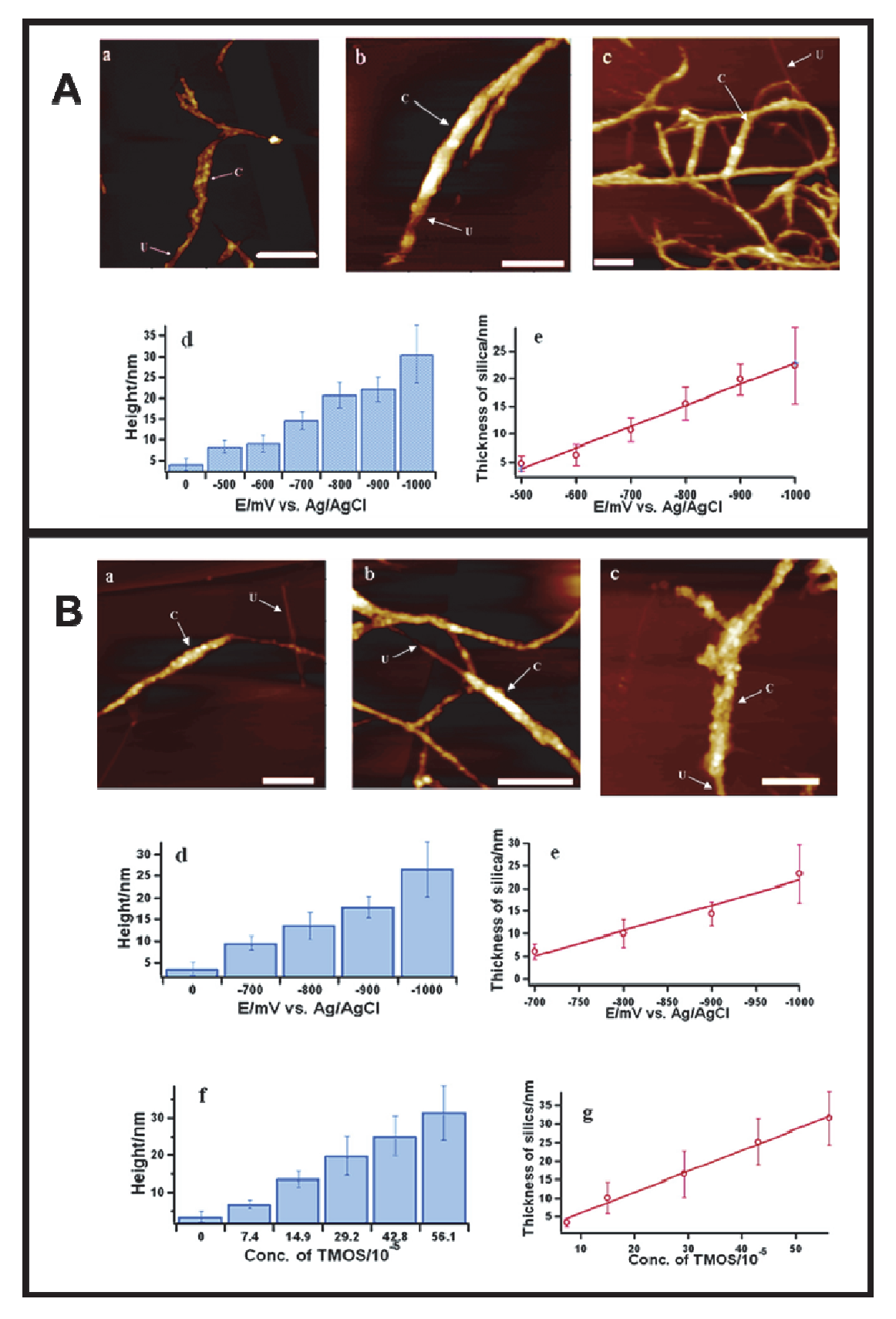


Figure 2.

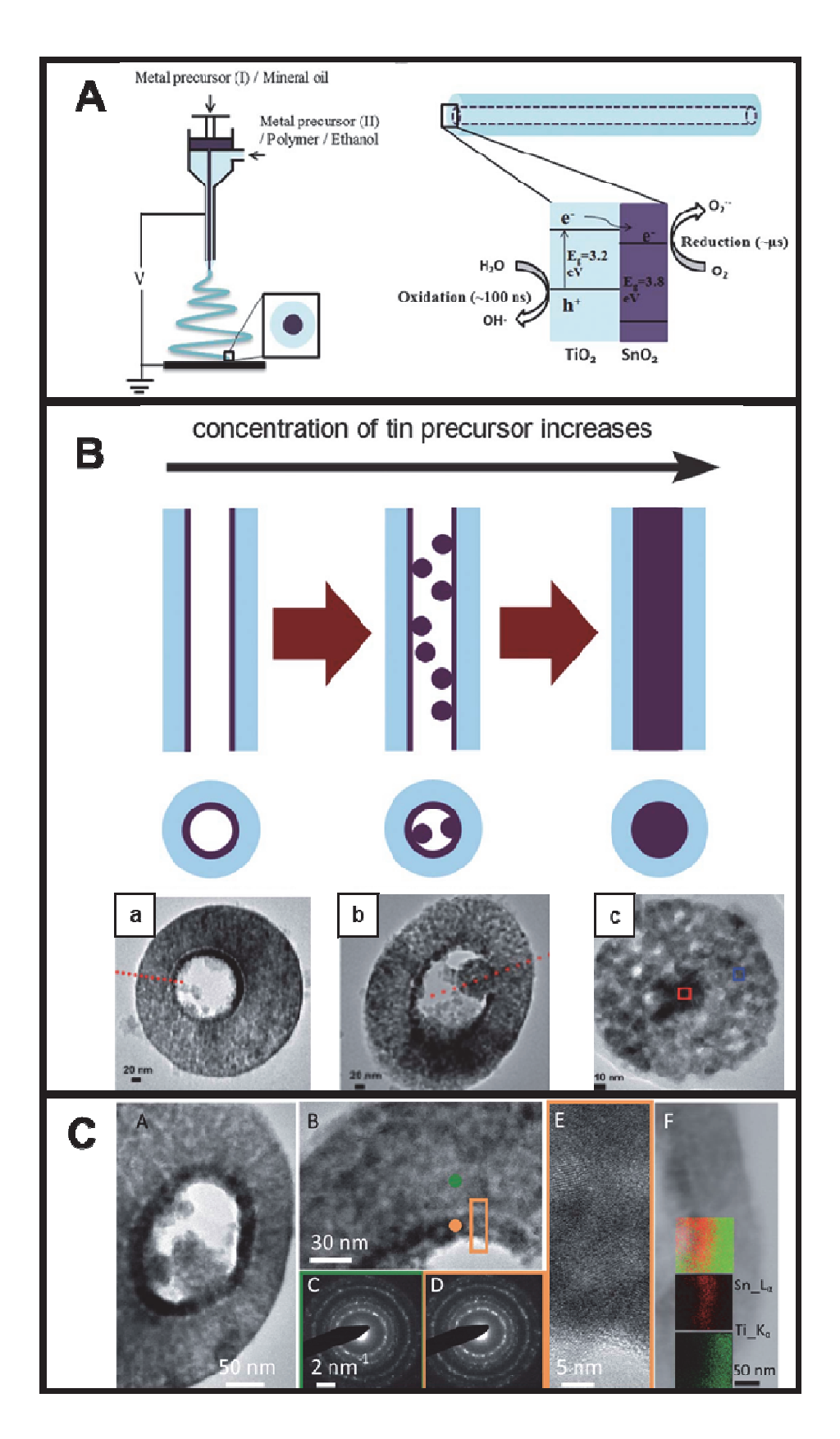


Figure 3.

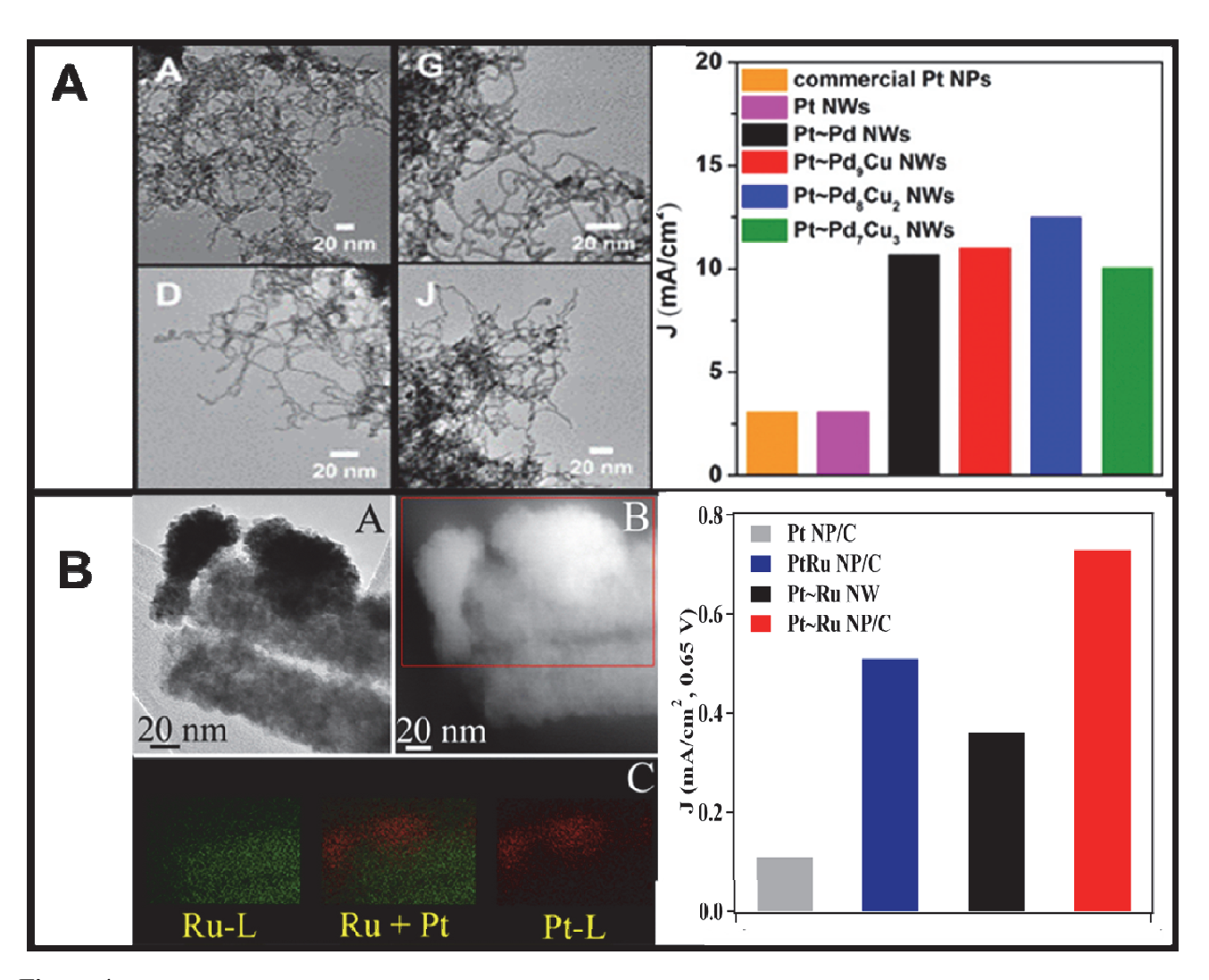


Figure 4.

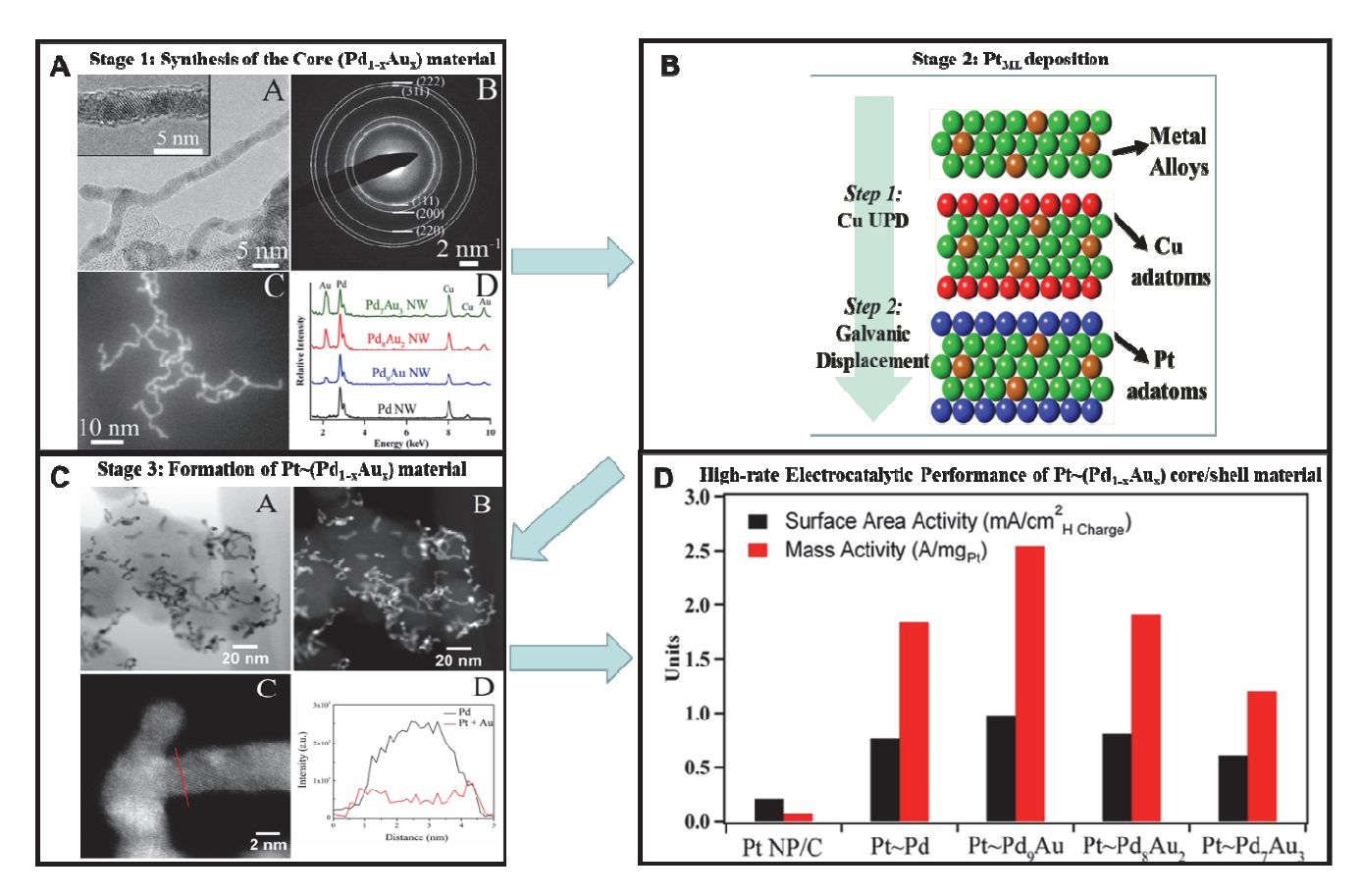


Figure 5.

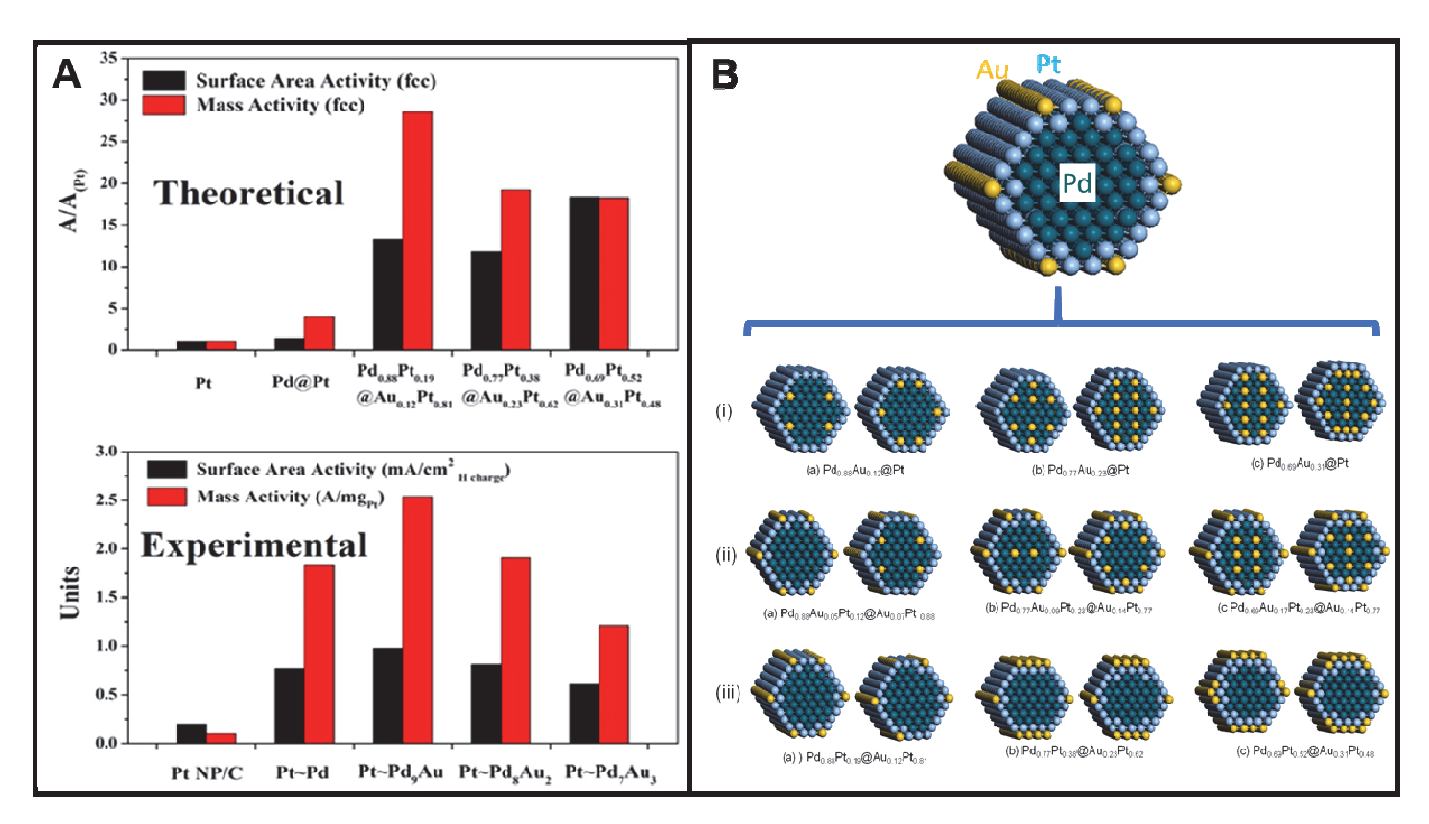


Figure 6.

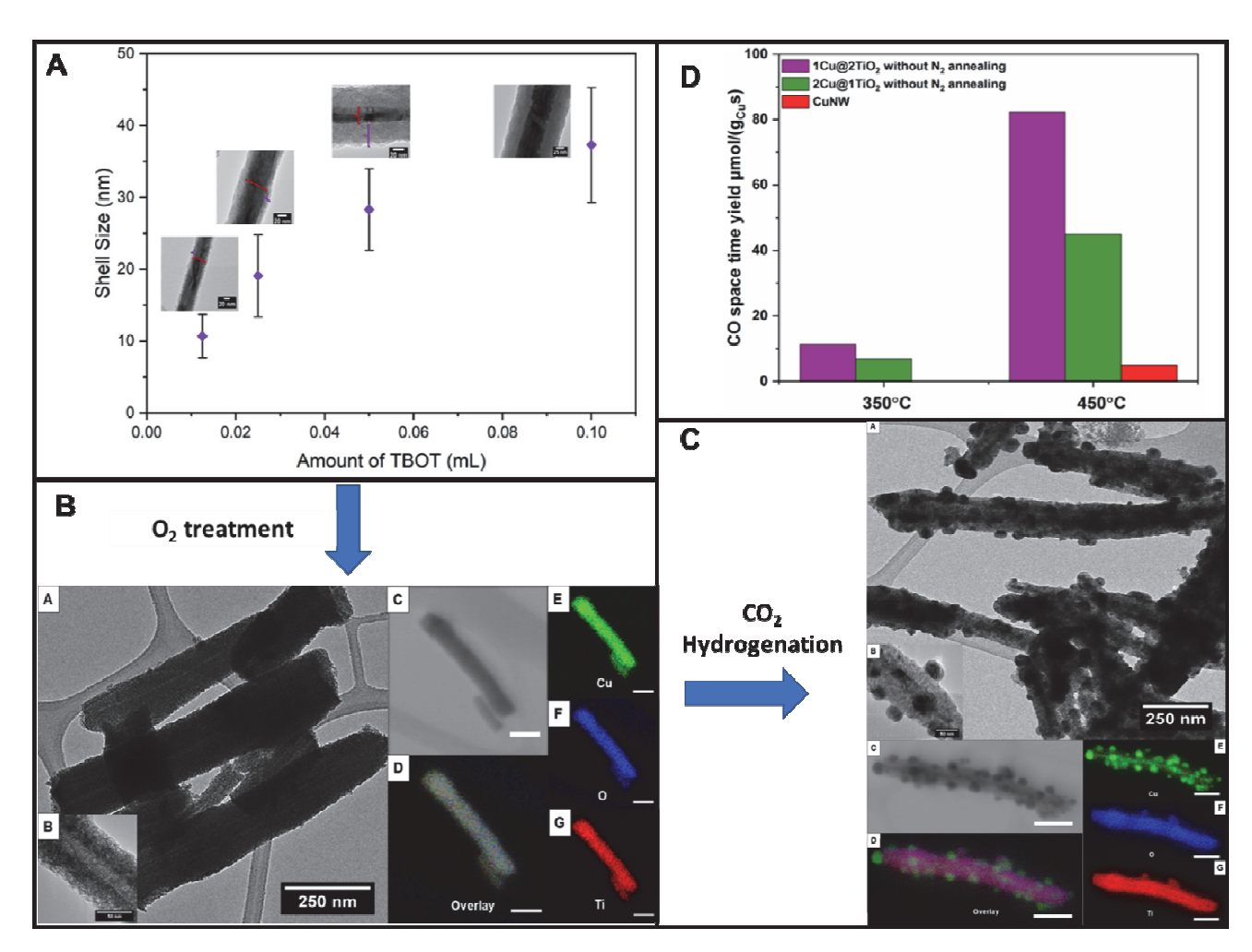


Figure 7.

Table 1. A Comparative Analysis of Synthesis Methods discussed in this Account.

Synthesis Method	Advantages	Disadvantages	Examples of Applications	Selected Key Parameters
Electro- deposition	 No surfactants or reducing agents¹⁴ Parameter control¹⁴ Precise and reproducible¹⁴ 	 Limited yields, as compared with standard deposition ¹⁴ Limited shell type composition Systems need to be conductive. ¹⁴ 	• Electrocatalysis ³³ • Fuel cells ¹⁴	 Magnitude of applied voltage Deposition time Precursor amounts
Electro- spinning	 Short reaction time¹⁸ High yield ¹⁸ Low cost¹⁶ Facile to implement¹⁶ Structure control¹⁶ 	 Dependent upon miscibility of the materials¹⁶ Materials must be chemically compatible.¹⁶ Potential for reduced yield, due to instrumental problems, such as nozzle clogging¹⁶ 	 Biomedicine¹⁶ Photocatalysis Drug delivery⁵³ Electrode generation⁵⁴ 	 Precursor amounts Feeding rate Magnitude of applied voltage
UPD/ Galvanic Displace- ment	 Precise control over shell thickness and uniformity¹⁴ Reproducible¹⁴ No surfactants or reducing agents¹⁴ 	 Requires conductive substrates¹⁹ More complicated than other wet chemical methods^{14,19} 	• Electrocatalysis ²	 Number of UPD/GD steps Potential used
Microwave -assisted Technique	 Facile to implement²¹ Short reaction time²¹ Allows for scaling up without thermal gradient effects²¹ Potential for high yield, purity, and reproducibility²² Green chemistry ²² 	 Wide distibution of seed nuclei,²¹ leading to product polydispersity Solvent must be either microwaveactive or possess a substantial dielectric constant²¹ Insufficient knowledge about growth mechanism²² 	• Gas sensing ²¹ • Thermocatalysis ¹ • Photocatalysis ²² • Electrocatalysis ²²	 Precursor